Steel Structures Research Update

Seismic Local Buckling Limits for Hollow Structural Section and Built-Up Box Columns

JUDY LIU

INTRODUCTION

Recently completed research on seismic local buckling limits for steel hollow structural section (HSS) and built-up box columns is featured. These National Center for Research on Earthquake Engineering (NCREE) studies are led by Dr. Chung-Che Chou and Dr. Tung-Yu Wu in the Department of Civil Engineering at National Taiwan University (NTU). Dr. Chou also serves as the NCREE Director. Dr. Chou's research has focused on seismic testing, analysis, and design for steel and post-tensioned self-centering structures. Some recent work includes studies on hybrid simulation of a full-scale steel moment frame, a post-tensioned self-centering brace, novel prediction models for early earthquake warnings, and earthquake reconnaissance work in eastern Taiwan. Dr. Chou's numerous accolades include the Awards for Excellent Research and Technology Transfers for his leadership on a research team developing a sandwiched buckling-restrained brace and a self-centering brace. Dr. Wu's research interests include collapse behavior of cold-formed HSS columns under seismic loading, subwavelength seismic metamaterial structures, crack growth in railway crossings under high wheel-rail impacts, and seismic resilience of steel buildings. In addition to multiple scholarships and fellowships, Dr. Wu's honors include the Raymond C. Reese Research Prize, awarded by the American Society of Civil Engineers (ASCE) for papers representing notable achievements in research with impact on design. The National Science and Technology Council is supporting this research on seismic local buckling limits for HSS and built-up box columns. Selected highlights from both projects are presented, along with a preview of future research tasks.

BACKGROUND AND OBJECTIVES

Seismic local buckling limits for HSS and built-up box columns have garnered interest due to some inconsistencies and conservatism. The seismic local buckling limits for HSS, for example, are quite different across seismic design codes in the United States, Japan, and Taiwan. The discrepancies are partially attributed to inconsistent loading protocols used in HSS research (Teng et al., 2023). Limits for HSS and built-up box columns have also been shown to be conservative (Lin and Chou, 2022; Teng et al., 2023). Through the featured research, complemented by concurrent studies led by Dr. Jason McCormick (University of Michigan) and Dr. Chia-Ming Uang (University of California–San Diego), Drs. Chou and Wu have been working to resolve these issues.

Research teams led by Drs. Chou and Wu aim to improve efficiency in HSS and built-up box column design through integrated experimental and computational studies focused on their seismic local buckling limits. Specific objectives for HSS and built-up box columns are to:

1. Characterize their seismic performance under combined axial and cyclic lateral loadings.
2. Extend the seismic performance knowledge base through a computational parametric study.
3. Evaluate the level of conservatism of the compactness requirements in existing seismic design provisions.
4. Propose highly and moderately ductile width-thickness limits.

HSS COLUMNS

A coordinated experimental-numerical investigation has provided insights into the seismic behavior of HSS columns. The experimental work demonstrated seismic performance relative to axial loading, element and member slenderness. Finite element simulations extended the work and aided in defining critical story-drift angles for the box columns. Revised seismic local buckling limits have been proposed based on this research.

Test Specimens, Test Setup, and Loading Protocol

Parameters investigated for six half-scale HSS columns included cross-section sizes, element width-to-thickness ratios, member slenderness, and grade of steel. The square HSS ranged from nominal 4 in. to 8 in. sections. Width and height dimensions, B and H, were 3.94 in., 5.91 in., 6.89 in.,

Judy Liu, PhD, Research Editor of the AISC *Engineering Journal*, Professor, Oregon State University, School of Civil and Construction Engineering, Corvallis, Ore. Email: judy.liu@oregonstate.edu\

and 7.87 in. Thickness, t, ranged from 0.236 in. to 0.472 in. For element slenderness, following the AISC *Specification* (2022a), 3 times the thickness, t, was subtracted from B and H to obtain b and h, the flat widths across each side. The resulting b/t and h/t values were 8.9, 14.9, 23.9, and 26.2. The element width-to-thickness ratio of 14.9 was evaluated for three nominal B and H values, allowing comparison for three different member slenderness values (i.e., length divided by radius of gyration, L/r). The ratio of 8.9 satisfies λ_{hd}, the width-to-thickness limit for a highly ductile member, while 14.9 satisfies λ_{md}, the limit for a moderately ductile member (AISC, 2022b). Most specimens were fabricated using steel grade STKR 490 with a specified minimum yield stress of 47.1 ksi. Similar to A500 grades, STKR490 HSS may be cold-formed from flat steel plate and welded. A design thickness of 0.93 times the nominal thickness was used in the b/t calculations. One specimen, with element width-to-thickness ratio of 26.2, used BCR 295 for tubes that were cold-formed from welded steel pipes, with a specified minimum yield stress of 42.8 ksi. The nominal thickness was used in the b/t calculations for BCR 295.

The specimens were subjected to axial compression and cyclic lateral loading. The Multi-Axial Testing System (MATS) shown in Figure 1 imposed fixed-fixed boundary conditions. For each specimen, a constant axial force, P, equal to 0.2 times the nominal axial yield force, P_y, was applied. The axial force was also reported in terms of P_{ya}, the yield strength calculated using the measured, or actual yield stress. The axial loading for these specimens ranged from 0.13 to 0.16 of P_{ya}. The cyclic lateral loading protocol of increasing displacements corresponding to increasing story-drift angles (e.g., 0.01, 0.02, 0.03 rad…) followed AISC *Seismic Provisions* Section K2 (AISC, 2022b).

Experimental Results

The test specimens exhibited overall similar behavior with differences in the hysteretic response. Local buckling was observed at the ends of the columns. The buckled shapes were either (1) outward at opposite sides and inward at the other opposite sides (Figure 2), or (2) outward at four sides. Figure 2 shows the first type of buckled shape for an STKR 490 specimen with $b/t = 23.9$ and $P/P_{ya} = 0.15$ in the second cycle of the 0.06 rad. A sample moment versus story-drift angle response is shown in Figure 3. The moment, M, has been normalized by the plastic moment capacity, M_{pc}, of the column. The results are for a nominal $6 \times 6 \times 0.25$ in.

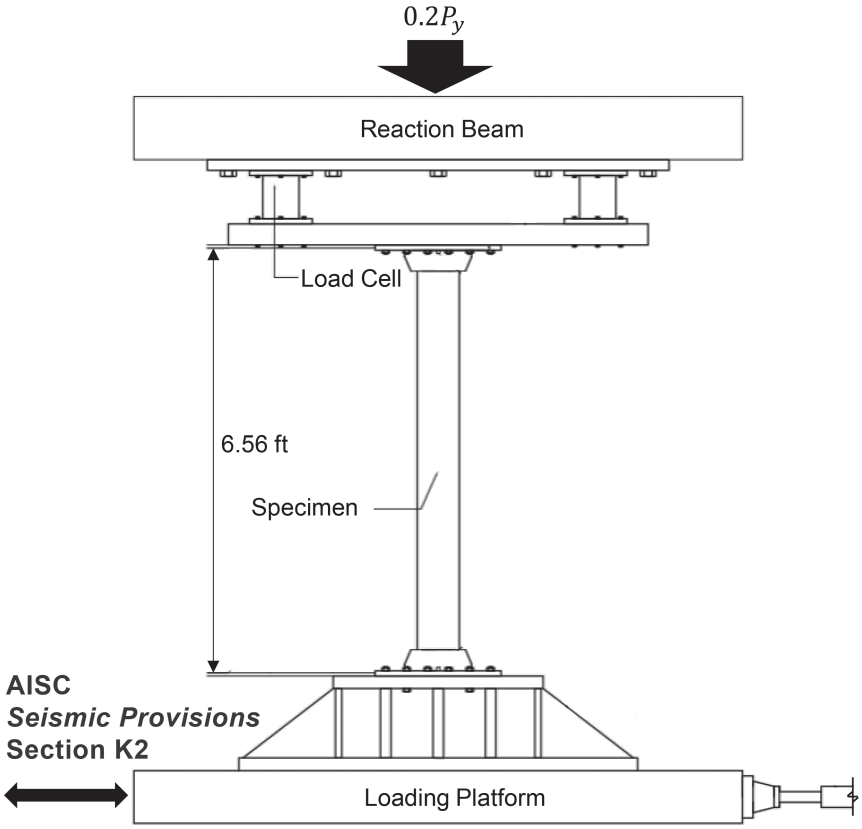

Fig. 1. Multi-Axial Testing System (MATS), shown here with HSS column specimen.

column with $b/t = 23.9$, $L/r = 34.2$, and $P/P_{ya} = 0.15$. Dashed lines in Figure 3 show the critical story-drift angle, SDA_{cr}, defined as the average of the story-drift angles (SDAs) corresponding to the positive and negative peak moment strength. The specimen has a $b/t = 23.9$ larger than $\lambda_{md} = 21.0$ but has an $SDA_{cr} = 0.03$; this is larger than expected ductility of 0.02 rad for a moderately ductile member. The tested specimens consistently exhibited better ductility than expected (e.g., 0.04 rad for a highly ductile member). The SDA_{cr} values ranged from 0.02 rad for a specimen with $b/t = 26.2$ to 0.09 for $b/t = 8.9$. The rest of the SDA_{cr} values were 0.03, 0.04, or 0.05. These results motivated the numerical investigation to follow.

Finite Element Simulation

Finite element simulations complemented the experimental test program. The finite element modeling approach corresponded to the experimental test setup and cyclic behavior of the HSS columns. Fully integrated shell elements and a nonlinear material model with kinematic hardening were used with the explicit solver in LS-DYNA (2013). Global and local geometric imperfections of $L/1500$ and $B/200$ were imposed (Figure 4). The columns were fully fixed at the bottom and fixed at the top except for lateral and vertical displacements.

The parameters for the computational study extended the experimental test program. An extensive analysis matrix included 33 sections of BCR 295 steel and 64 sections of BCP 325 steel. BCR 295 uses the cold-roll-forming process, and BCP 325 uses a cold-press process (Takeshi and Takuya, 2020). Each column was analyzed for three different P/P_y ratios (0.2, 0.3, 0.4), totaling 291 numerical simulations.

The numerical simulation results were used to extend the experimental test program and explore alternative seismic local buckling limits. The column results were plotted with respect to b/t and P/P_{ya} (Figure 5). Figure 5, with results for BCR 295 steel, shows how the SDA_{cr} changes with b/t and P/P_{ya}. The results are also compared to current moderately ductile, λ_{hd}, and highly ductile, λ_{hd}, limits, shown with dashed lines. Multivariate regression analysis was used to develop an SDA_{cr} equation with input parameters b/t, P/P_{ya}, and F_{ya}/E, where F_{ya} is the yield stress and E is the elastic modulus. The results were also modified for the effects of boundary conditions and loading protocol, following the

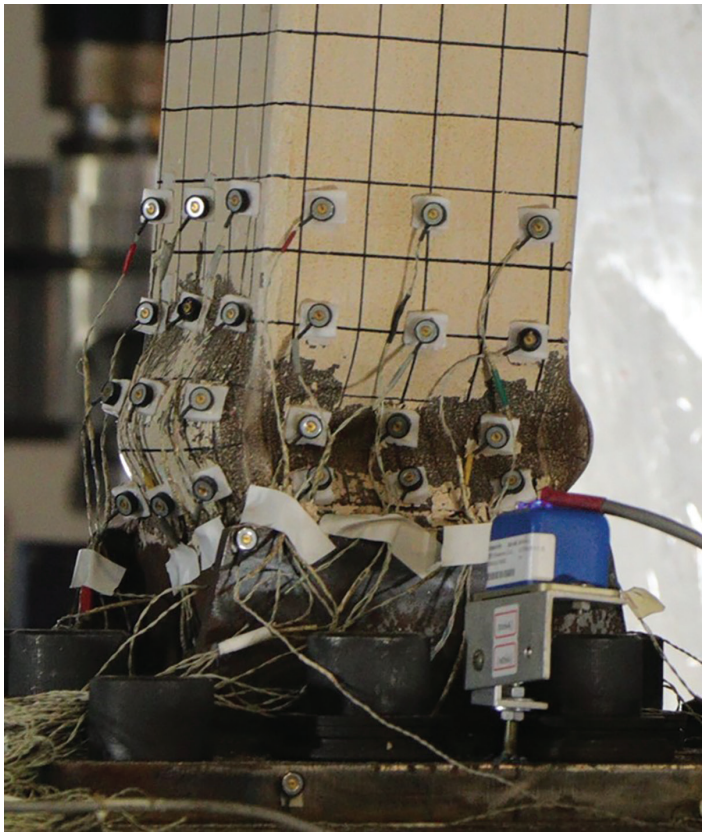

Fig. 2. Common failure mode of HSS columns—inward flange buckling and outward web buckling (photo is for a test specimen with $b/t = 23.9$, $P/P_{ya} = 0.15$, *0.06 rad, 2nd cycle).*

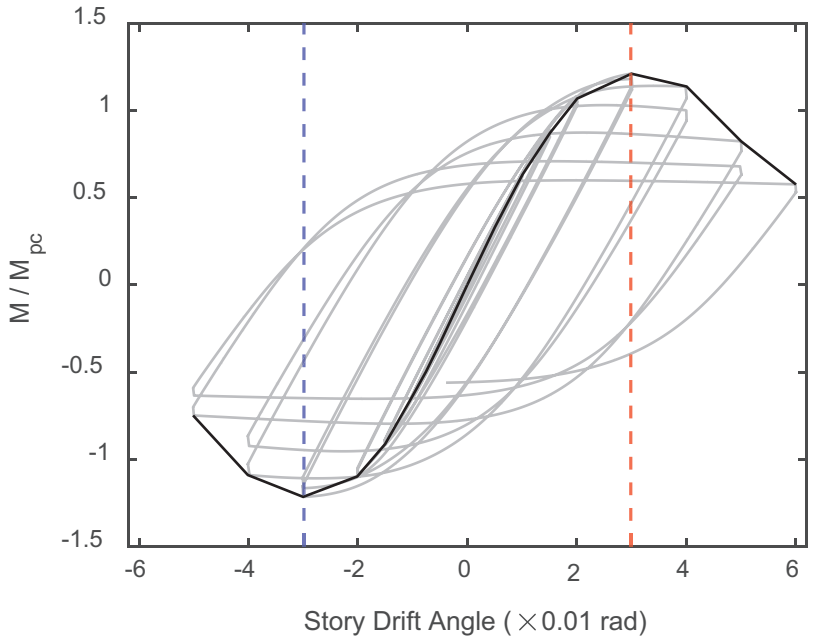

Fig. 3. Hysteretic response of nominal 6 × 6 × 0.25 in. specimen ($b/t = 23.9$, $L/r = 34.2$, *and* $P/P_{ya} = 0.15$*).*

(a) 3D view *(b) Global imperfection shape* *(c) Local imperfection shape*

Fig. 4. Finite element model of HSS columns.

work of Ozkula et al. (2021) to define adjusted critical story drift angles, or SDA'_{cr}.

Development of Seismic Local Buckling Limits

A few steps are needed for the transition from adjusted critical story-drift angle, or SDA'_{cr}, to seismic local buckling limits. First, the SDA'_{cr} values are set to performance targets for moderately and highly ductile members. SDA'_{cr} is defined as 0.02 rad for a moderately ductile column in an intermediate moment frame (IMF) and 0.04 rad for a highly ductile column in a special moment frame (SMF). Rewriting the SDA'_{cr} equations to define the b/t values provides equations for the moderately ductile, λ_{md}, and highly ductile, λ_{hd}, limits. Figure 6 compares proposed limits to those in the current AISC *Seismic Provisions* (2022b). The proposed highly and moderately ductile limits are in terms of C_a, a ratio between the factored axial load demand and the expected yield capacity of the column.

BUILT-UP BOX COLUMNS

The built-up box column research was another investigation that integrated experimental testing with computational simulations. The work was motivated by and extended previous research on the seismic behavior of built-up box columns. The beam-to-column subassemblage tests and finite element simulations further extended the work with characterization of boundary condition and near-fault loading effects for defining critical story-drift angles for the box columns. Revised seismic local buckling limits have been proposed based on this research.

Previous Testing on Built-Up Box Columns

Prior research on built-up box columns has informed current research efforts. Tests have been conducted on isolated columns, subassemblages, and full frames. The research has revealed some conservatism in the current seismic local buckling limits and provided direction for research underway.

Cyclic work of isolated columns has shown differences between wide-flange and built-up box columns, as well as potential improvements for box columns. Chou and Chen (2020) tested six large-scale, built-up box columns with fixed-fixed boundary conditions. Four columns were subjected to a constant axial load ($0.25–0.4P_y$) and cyclic lateral loading, and another two columns were subjected to a constant axial load ($0.4P_y$) and different near-fault lateral loadings. The columns performed well at high lateral drifts when the column satisfied the width-thickness limit for highly ductile members, λ_{hd} (AISC, 2022b). Lin and

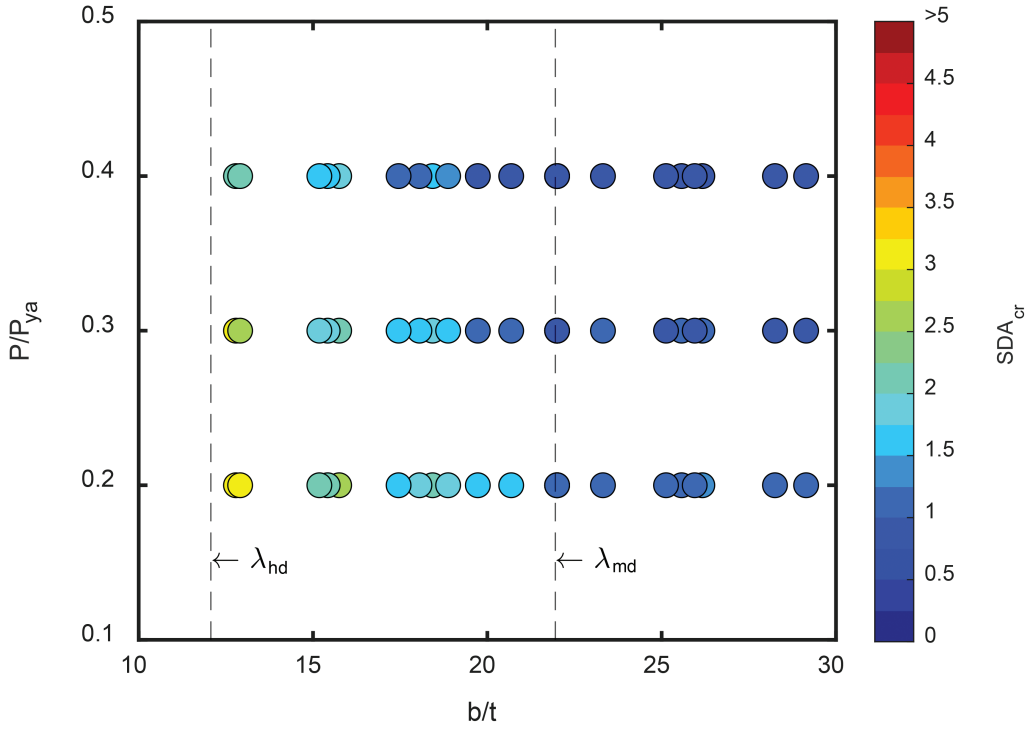

Fig. 5. Critical story drift angle (SDA_{cr}) of considered BCR295 sections.

Chou (2022) further tested deep wide-flange columns and built-up box columns, all satisfying the highly ductile member requirement, λ_{hd}. The work showed that (1) the AISC *Seismic Provisions* λ_{hd} limit results in markedly different cyclic responses for deep wide-flange columns and built-up box columns, and (2) the highly ductile member requirement, λ_{hd}, for built-up box columns is overly conservative.

The boundary conditions greatly influence column cyclic behavior. In multistory buildings, the connections and continuation to the beams and columns at the second story affect the lateral stiffness and deformation capacity of first-story columns. Chou et al. (2023) studied the first-story column behavior by adopting actual boundary conditions in steel multistory buildings. The first-story built-up box column tests were conducted by using a half-scale, beam-to-column subassemblage consisting of a two-and-a-half-story steel frame with I-shaped beams at two floors. Figure 7 shows the frame, a test specimen at 0.045 rad drift, and the column deformations at that level of drift. No yielding or buckling was observed at the top ends of the first-story columns. However, yielding at the bottom ends of the second-story columns was observed at medium lateral drifts for the highly ductile built-up box column because the strong column–weak beam (SCWB) requirement was met by a small margin based on the AISC *Seismic Provisions* (AISC, 2022b).

The boundary conditions and other parameters were studied in additional subassemblage tests. To further investigate the cyclic behavior of first-story built-up box columns under reversed cyclic lateral loading and constant axial loading, Chou et al. (2024a) conducted tests on subassemblage columns by using a full-scale, one-and-a-half-story subassemblage testing scheme (Figure 8). The columns had different width-thickness ratios (16.2 and 20.5) and axial load ratios ($0.25P_y$ and $0.4P_y$). Four subassemblages were designed with steel beams at the second floor and a moderately ductile built-up box column. All were able to achieve at least one complete test cycle at 0.04 rad drift without noticeable degradation in strength. Figure 8 shows a test specimen and the column local buckling at 0.05 rad lateral drift. By collecting moment and drift data at 0.02 and 0.04 rad from isolated column and subassemblage column tests, a relaxed b/t limit for the flange of highly ductile built-up box sections, $\lambda_{hd} = 0.96\sqrt{E/R_yF_{yn}}$, was proposed, significantly exceeding the current limit in (AISC, 2022b). Moreover, one additional subassemblage was tested using the hybrid simulation of a full-scale, seven-story steel dual frame, verifying the acceptable seismic performance of the moderately ductile built-up box column under varying axial compression load ($0.11–0.38P_y$) and lateral drifts to 1.5 times the maximum considered earthquake level (Wang et al., 2023).

Shake table tests complemented the experimental work on built-up box columns. Evaluating the seismic performance of moderately ductile built-up box columns in earthquakes, Chou et al. (2024b), conducted shake table tests on a full-scale, three-story steel dual frame (Figure 9) with a buckling-restrained braced frame and a special moment frame. The test results indicated that the b/t requirement for highly ductile built-up box columns in the AISC *Seismic Provisions* (2022b) is overly conservative. Columns with a large b/t value (e.g., 21), exceeding the highly ductile column requirement (λ_{hd} = 12.2), still provided satisfactory performance in the first story at large drifts without showing strength degradation (i.e., 0.038 rad).

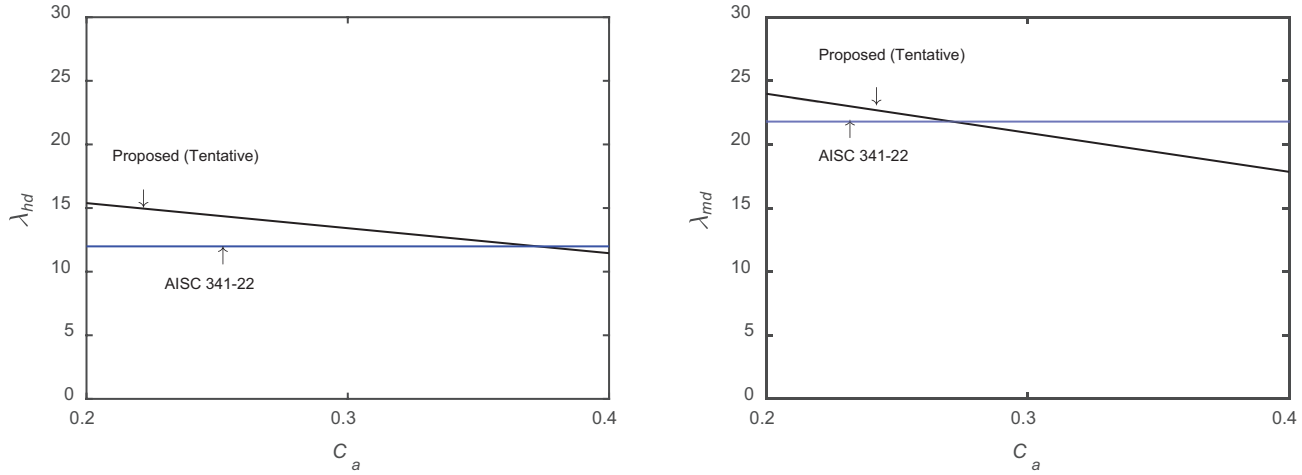

(a) Highly ductile *(b) Moderately ductile*

Fig. 6. Proposed highly and moderately ductile limits compared with current limits in the AISC Seismic Provisions.

Fig. 7. Two-and-a-half-story steel beam-to-column subassemblage: (a) prototype frame, (b) deformation at 0.045 rad lateral drift, and (c) column deformation after 0.045 rad lateral drift.

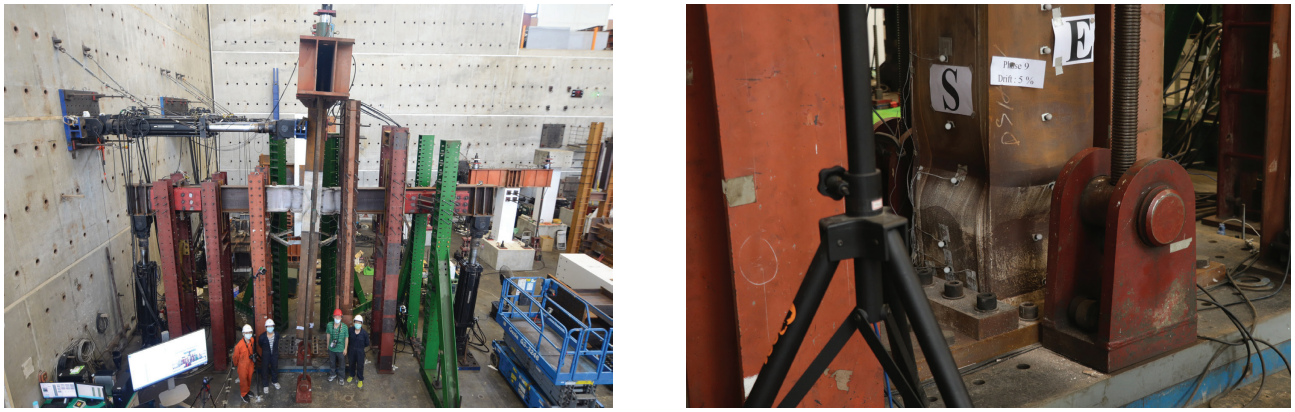

Fig. 8. One-and-a-half story steel beam-to-column subassemblage: (a) deformation at 0.05 rad lateral drift and (b) column local buckling after 0.05 rad lateral drift.

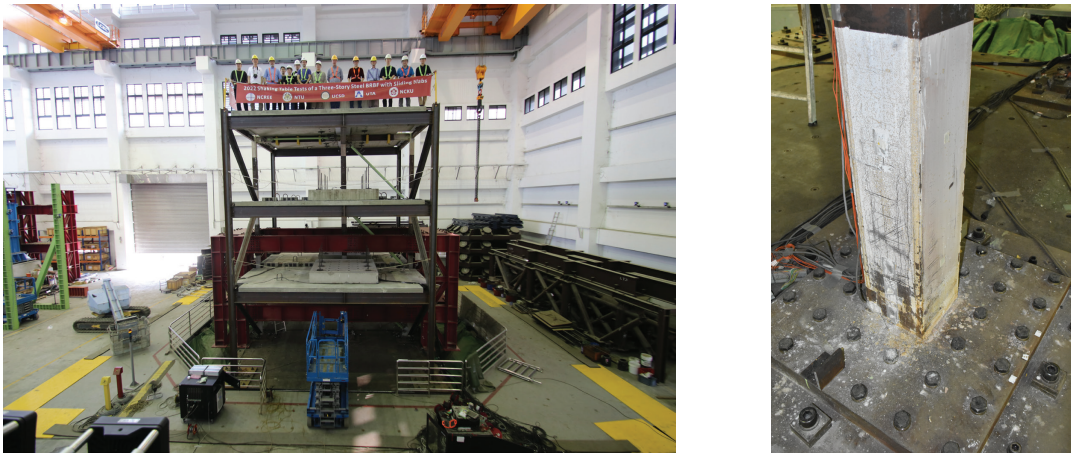

Fig. 9. Shake table testing of a steel (a) three-story dual system and (b) a column base after testing (2.7MCE level).

Test Specimens, Setup, and Loading Protocol

The research team has conducted cyclic lateral tests on 10 square built-up box columns with varying element slenderness and axial loading. Four of the tests were from the previous study by Chou and Chen (2020). The walls of the box columns were joined by complete-joint-penetration (CJP) groove welds as shown in Figure 10. The SN 490B steel had a specified minimum yield stress of 47.1 ksi. Outside dimensions for the specimens ranged from 12 to 16 in., and thicknesses ranged from 0.5 to 1.125 in. The resulting width-thickness (b/t) ratios were from 11.8 to 36. Ratios lower than 15.4 satisfy λ_{hd}, the width-to-thickness limit for a highly ductile member, while ratios lower than 23.7 satisfy λ_{hd}, the limit for a moderately ductile member (AISC, 2022b). The 2020 specimens included two highly ductile and two moderately ductile columns. The remaining specimens, tested in 2024, all exceeded the moderately ductile member limit. The specimens were subjected to axial compression and cyclic lateral loading. The Multi-Axial Testing System (MATS) (Figure 1) was used to impose the loading and fixed-fixed boundary conditions. These columns were subjected to a constant axial load of 0.2 to 0.4 times the axial yield capacity. Cycles of increasing lateral drift were applied following the standard loading protocol of the AISC *Seismic Provisions* (AISC, 2022b) for testing special moment connections.

Experimental Results

As with the HSS columns, the built-up box columns exhibited overall similar behavior with differences in the hysteretic response. Local buckling was observed at the ends of the columns. Flange fracture close to the CJP weld also occurred in the 2024 box columns. Axial load effects can be seen in the moment versus rotation results. Figure 11 shows moment-rotation plots for columns with the same b/t but twice the axial load for one of the specimens. The higher axial load results in a lower peak moment and deformation capacity. Trends with b/t values were also observed.

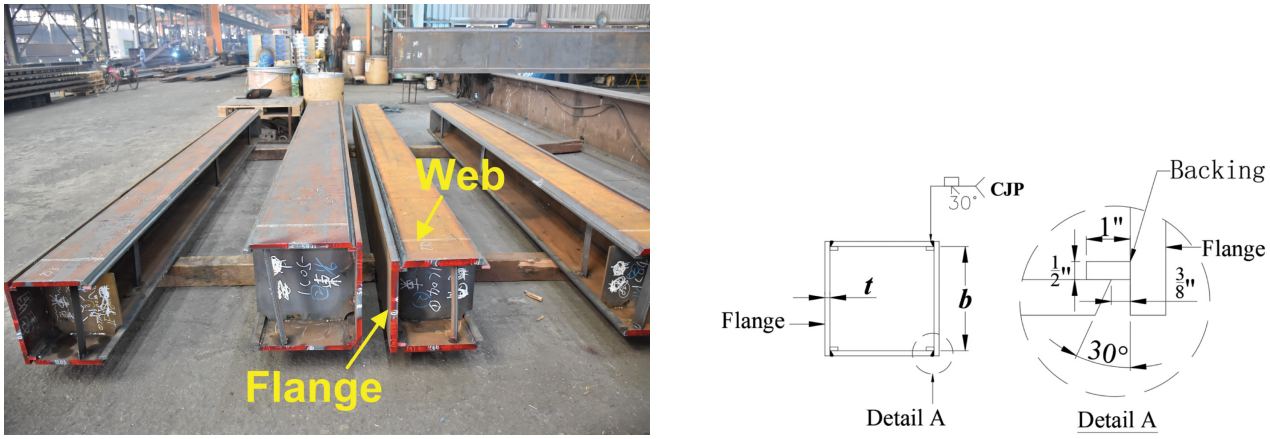

(a) In fabrication *(b) Complete-joint-penetration (CJP) groove welds*

Fig. 10. Built-up box column assembly.

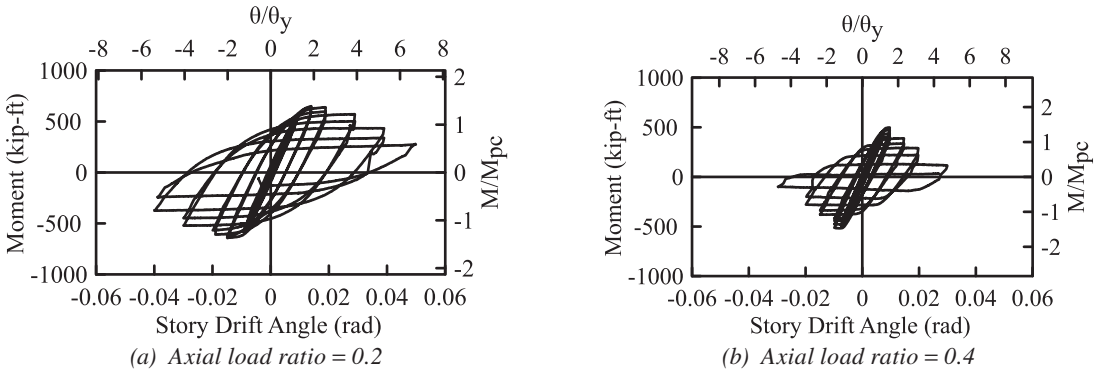

(a) Axial load ratio = 0.2 *(b) Axial load ratio = 0.4*

Fig. 11. Moment-rotation responses for built-up columns with b/t = *36.*

The first four columns (Chou and Chen, 2020) performed well with SDA_{cr} values of 0.03 and 0.04, the latter for those satisfying the highly ductile member requirement λ_{hd} in the AISC *Seismic Provisions* (AISC, 2022b). The next six columns, which exceeded the moderately ductile limit, exhibited lower ductility (e.g., SDA_{cr} values from 0.01 to 0.02) and strength degradation.

Finite Element Simulations

Subassemblage test results were used to characterize a boundary condition factor on the isolated columns. Finite element analysis program ABAQUS (2016) was used to characterize loading effects (cyclic versus near-fault loadings) on the isolated columns. The team developed models of the test specimens, subjected them to the same loading protocols, and compared the experimental to the computational results (Figure 12). The observed local buckling and moment-rotation results compared well between the physical experiments and the computational simulations. Finite element comparisons were also made between the fixed-fixed isolated columns under the standard cyclic loading of the AISC *Seismic Provisions* and the near-fault loading from Lin and Chou (2022) to develop a loading factor. The two factors were used to define the adjusted critical story-drift angle, or SDA'_{cr}, with modifications of the isolated column test results for boundary conditions and loading protocol effects (Ozkula et al., 2021).

Development of Seismic Local Buckling Limits

The research results have been used to develop proposals for seismic local buckling limits for square, built-up box columns. Following the methodology for I-shaped deep

(a) Local buckling in the experiment

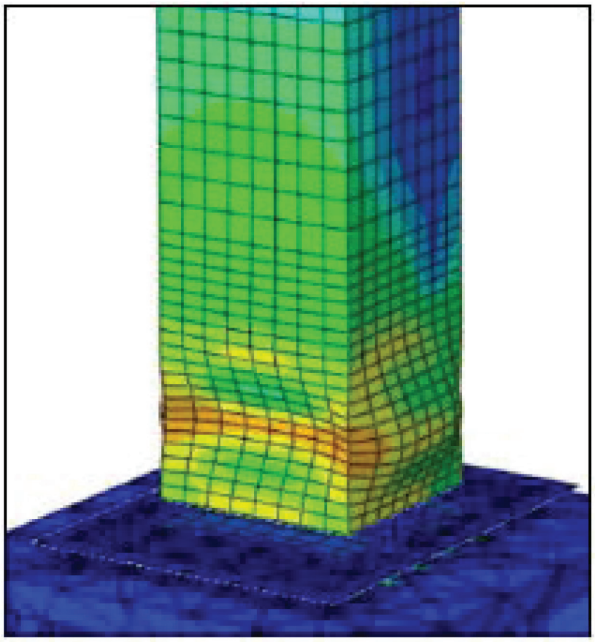

(b) Local buckling observed in FEA

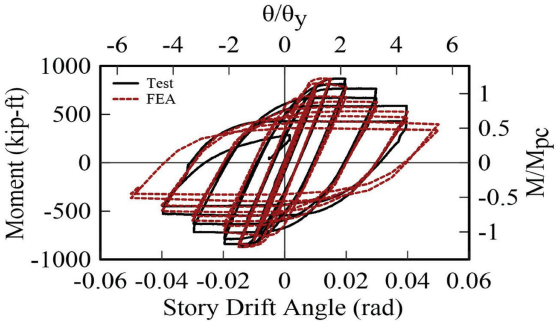

(c) Comparison of the experimental versus finite element analysis moment-rotation results

Fig. 12. Sample isolated column.

columns (Ozkula et al., 2021), the team proposed preliminary revised seismic b/t limits that are dependent on the column axial load ratio (Figure 13). Figure 13 shows the proposed highly and moderately ductile limits in terms of C_a, a ratio between the factored axial load demand and the expected yield capacity of the column. Comparisons to the current AISC limits (AISC, 2022b) are also shown. The experimental results had indicated that the current highly ductile and moderately ductile b/t limits for square built-up box members in the AISC *Seismic Provisions* are too conservative except for the columns under a very high constant axial load (0.4–0.5 times the axial yield capacity). The proposed limits capture the axial load effect and remove the conservatism for lower axial loads.

FUTURE WORK

The featured work has focused on the seismic performance of square HSS and built-up box columns. Cyclic testing included isolated HSS and box columns, as well as subassemblage and shake table testing for the built-up box columns. Previous work had found some member width-to-thickness limits to be too conservative. The investigations presented here resulted in preliminary proposals for revised seismic b/t limits. Future research needs include investigation into the observed fracture of CJP groove welds caused by severe buckling in the built-up box columns. Future work may also include tests with bi-directional lateral loading together with axial load on the column. The researchers would like to extend the half-scale HSS work with full-scale experiments to further verify the simulation results and the proposed equations. Differences across steel grades (e.g., A500, A1085, STKR, BCR) may also be studied. Meanwhile, future work plans include similar studies of non-square HSS and built-up box column members with different width-to-thickness ratios for webs and flanges.

ACKNOWLEDGMENTS

Thank you to Dr. Chou and Dr. Wu for all the materials, coordination, edits, and other feedback and contributions. The contributions of Nicholas Tedjasukmana, Guan-Wei Chen, Hou-kan Sen, Chien-Ting Weng, and Yu-Wen Teng of NTU and Chi-Rung Jian (NCREE) are also acknowledged. The research is sponsored by the National Science and Technology Council, Taiwan. The researchers would also like to thank collaborators Dr. Jason McCormick (University of Michigan) and Dr. Chia-Ming Uang (University of California–San Diego). Any findings or recommendations are those of the researchers and do not necessarily reflect the views of the sponsors.

REFERENCES

ABAQUS (2016), *ABAQUS/CAE User's Guide 6.13*, Dassault Systemes Simulia Corporation, Waltham, Mass.

AISC (2022a), *Specification for Structural Steel Buildings*, ANSI/AISC 360-22, American Institute of Steel Construction, Chicago, Ill.

AISC (2022b), *Seismic Provisions for Structural Steel Buildings*, ANSI/AISC 341-22, American Institute of Steel Construction, Chicago, Ill.

Chou, C.-C. and Chen, G.-W. (2020), "Lateral Cyclic Testing and Backbone Curve Development of High-Strength Steel Built-Up Box Columns under Axial Compression," *Engineering Structures*, Vol. 223, 111147.

Chou, C.-C., Lin, H.-Z., Córdova, A., Chen, J.-M., Chou, Y.-H.D., Chao, S.-H. Chao, S.-H., Tsampras, G., Uang, C.-M., Chung, H.-Y., Loh, C.-H., and Hu, H.-T. (2024b), "Earthquake Simulator Testing of a Three-Story Steel Building for Evaluating Built-Up Box Column Performance and Effect of Sliding Slab," *Earthquake Engineering and Structural Dynamics*, https://doi.org/10.1002/eqe.4130.

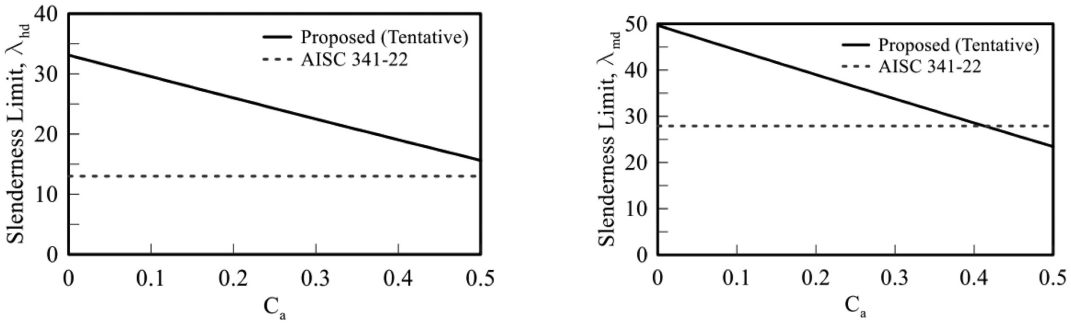

(a) Highly ductile *(b) Moderately ductile*

Fig. 13. Preliminary revised seismic b/t *limits.*

Chou, C.-C., Shen, H.-K., and Chou, Y.-H.D. (2024a), "Subassemblage Test and Width-Thickness Design Limit for Steel Built-Up Box Columns Subjected to Axial Load and Cyclic Lateral Drift," *Engineering Structures*, Vol. 308, 118023.

Chou, C.-C., Xiong, H.-C., Kumar, A., Lai, Y.C., and Uang, C.M. (2023), "Effects of Section Compactness and SCWB Condition on Moment Redistribution and Plastic Hinging in SMF Built-up Box Columns," *Journal of Structural Engineering,* ASCE, Vol. 149, No. 11, 04023144.

Lin, T.-H. and Chou, C.-C. (2022), "High-Strength Steel Deep H-Shaped and Box Columns under Proposed Near-Fault and Post-Earthquake Loadings," *Thin-Walled Structures*, Vol. 172, 108892.

LS DYNA (2013), *LS-DYNA Keyword User's Manual*, Livermore Software Technology, Livermore, Calif.

Ozkula G., Uang C.-M., and Harris J. (2021), "Development of Enhanced Seismic Compactness Requirements for Webs in Wide-Flange Steel Columns," *Journal of Structural Engineering*, ASCE, Vol. 147, No. 7.

Takeshi, I. and Takuya, M. (2020, March), "Overview of Construction Products and Methods in JFE Group," JFE Technical Report, No. 25, JFE Steel Corporation.

Teng, Y.-W., Wu, T.-Y., Weng, C.-T., and Jiang, C.-R. (2023), "Seismic Performance of Square HSS Columns," *34th KKHTCNN Symposium on Civil Engineering*, Pattaya, Thailand. (abstract only).

Wang, K.-J., Chou, C.-C., Huang, C.-W., Shen, H.-K., Sepulveda, C., Mosqueda, G., and Uang, C.-M. (2023), "Hybrid Simulation of a Steel Dual System with Buckling-Induced First-Story Column Shortening: A Mixed Control Mode Approach," *Earthquake Engineering and Structural Dynamics*, Vol. 52, No. 12, pp. 3,727–3,745. DOI: 10.1002/eqe.3944.